Jacquemin, F., **Fréour, S.,** Guillén, R. (2006). Analytical Modeling of Transient Hygro-elastic Stress Concentration - Application to embedded optical fiber in a non-uniform transient strain field, *Composites Science and Technology*, **66**, 397-406.

Analytical Modeling of Transient Hygro-elastic Stress Concentration

- Application to embedded optical fiber in a non-uniform transient strain field -

F. Jacquemin*, S. Fréour and R. Guillén

Institut de Recherche en Génie Civil et Mécanique (UMR CNRS 6183),

IUT de Saint-Nazaire - Université de Nantes,

37 Boulevard de l'Université, BP 406, 44 602 Saint-Nazaire cedex, France.

Abstract

The aim of this work is to propose an analytical model for transient hygro-elastic stresses in transversely isotropic multi-layered cylinders. This approach allows to calculate the time and space dependent hygro-elastic stresses in fiber-reinforced composite submitted to hygroscopic fields by applying the classical continuum mechanics formalism. Application of the proposed model to the case of an embedded optical fiber shows interesting results, concerning the stress field perturbation occurring in the composite in the vicinity of the intrusive optical fiber. The model proposed in this study provides a detailed stress analysis of the inclusion which is required to correctly interpret the data collected through the optical fiber and deduce stresses experienced by the host material.

Keywords: A. Fibres; A. Layered structures; B. Hygrothermal effects; C. Residual stress; D. Stress concentration

*Corresponding author :
Fax number : +33240172618
E-mail address: frederic.jacquemin@univ-nantes.fr (F. JACQUEMIN)

1. Introduction

Thermal stress and strain analyses have been performed in unidirectional fiber-reinforced composites by considering the concept of concentric cylinders. Various theoretical expressions [1-5] exist for the principal (radial, circumferential and longitudinal) stresses in the fibers and the matrix and at the interface between them. Nairn [2] studied the case where only the central cylinder – that is, the fiber – is transversely isotropic. More recently, Wagner and Nairn [3] and Anifantis et al. [4] have extended this approach to predict the thermal stresses in fiber-reinforced composite materials containing transversely isotropic interphases and/or matrices. These investigations do not incorporate a transient non-uniform thermal field in the analysis: stresses result from a uniform temperature change only. Nevertheless, in practice, internal stresses arise from thermal change and/or hygroscopic change usually encountered during the service life of the composite structures. Furthermore, in the literature there is no model dealing with transient non-uniform hygrothermal problem. The model used in this study is the classical composite cylinder model extended to the transient hygro-elastic case. This analytical approach consists in concentric hollow cylinders with transversely isotropic homogeneous materials defined in each separate cylinder. In the present work, we performed a two-dimensional transient-state hygro-elastic analysis of multi-layered materials. Application of the proposed model to the case of an embedded optical fiber shows very interesting results, concerning the stress field perturbation occurring in the composite in the vicinity of the optical fiber. In fact, Optical Fiber Bragg Gratings (FBG) sensors offer an indispensable tool to study, in a minimally invasive manner, internal strains in polymeric materials: up to now, FBG have been used to measure thermal strains but also constitute a

pertinent way to analyse moisture induced strains (even if, to the author knowledge, no paper in the literature deals with this topic).

2. Two concentric cylinders

First, consider two concentric cylinders only (Figure 1), the central one being the transversely isotropic material 1, and the other being the transversely isotropic material 2. Perfect interfacial bonding is assumed between the cylinders. A hygro-elastic model for multi-layered materials subjected to transient moisture content is investigated. Moreover, the moisture contents of the materials can be strongly different. As example, the model is used to simulate the presence of an optical fiber (material 1), considered not to absorb water, embedded in an unidirectional fiber-reinforced composite (material 2) in order to measure its hygro-elastic stress state. In order to predict the reliability of the measurement with optical fibers and to prevent a possible damage occurrence generated not by the ambient conditions but by the embedded optical fiber, it is necessary to estimate the perturbations occurring in the composite stress field due to the presence of the optical fiber.

The assembly composed of materials 1 and 2 is supposed initially dry. Then, the external material is exposed to an ambient fluid with boundary moisture content m_0. The moisture content is solution of the following system with unidirectional Fick's law (1), where D is the transverse diffusion coefficient of the composite. The moisture flux is assumed to be null at the interface between the material 1 and the material 2 because the material 1 does not absorb water.

$$\frac{\partial m}{\partial t} = D\left[\frac{\partial^2 m}{\partial r^2} + \frac{1}{r}\frac{\partial m}{\partial r}\right] \quad a<r<b,\ t>0 \tag{1}$$

$$\begin{cases} \dfrac{\partial m(a,t)}{\partial r} = 0 \\ m(b,t) = m_0 \\ m(r,0) = 0 \end{cases} \tag{2}$$

According to [6], the time and space dependent moisture content, *m(r,t)*, solution of the problem (1)-(2) is:

$$m(r,t) = m_0\left[1 + \pi \sum_{m=1}^{\infty} \frac{\exp(-D\omega_m^2 t)}{J_0^2(b\omega_m) - J_1^2(a\omega_m)} J_1^2(a\omega_m)\{Y_0(b\omega_m)J_0(r\omega_m) - J_0(b\omega_m)Y_0(r\omega_m)\}\right] \tag{3}$$

with ω_m the mth positive root of: $J_0(b\omega_m)Y_1(a\omega_m) - J_1(a\omega_m)Y_0(b\omega_m) = 0$

where J_0, J_1, Y_0 and Y_1 are Bessel's functions of first or second kind.

2.1. Mechanical Problem

At the initial time, the cylinders are assumed to be stress free. Therefore, the hygroelastic orthotropic behaviour writes as follows in (4), where $\boldsymbol{\beta}$ and $\mathbf{L}$ are respectively the in-plane tensors of hygroscopic expansion coefficients and elastic moduli. Those tensors are assumed to be material constants.

$$\begin{Bmatrix} \sigma_{11} \\ \sigma_{22} \\ \sigma_{33} \end{Bmatrix} = \begin{bmatrix} L_{11} & L_{12} & L_{12} \\ L_{12} & L_{22} & L_{23} \\ L_{12} & L_{23} & L_{22} \end{bmatrix} \begin{Bmatrix} \varepsilon_{11} - \beta_{11}\Delta m \\ \varepsilon_{22} - \beta_{22}\Delta m \\ \varepsilon_{33} - \beta_{22}\Delta m \end{Bmatrix} \tag{4}$$

Solving the hygro-mechanical problem, requires to express the strains versus the displacements (5) along with the compatibility and equilibrium equations (6).

$$\left\{\varepsilon_{33}=\frac{\partial w}{\partial r},\quad \varepsilon_{22}=\frac{w}{r},\quad \varepsilon_{11}=\frac{\partial u}{\partial x}.\right. \tag{5}$$

$$\frac{\partial \sigma_{33}}{\partial r}+\frac{\sigma_{33}-\sigma_{22}}{r}=0 \tag{6}$$

The displacement component in the longitudinal direction *u(x)* is then deduced:

$$\begin{cases} u(x)=Ax \\ A \text{ is a constant} \end{cases} \tag{7}$$

It is worth noticing that the displacement *u(x)* does not depend on the moisture content field. Finally, to obtain the through-thickness or radial component of the displacement *w*, we shall consider in the following the analytical transient moisture content (3).The radial component of the displacement field in the material 2, denoted $w^{(2)}$, satisfies the following equation:

$$\begin{cases} r^2\dfrac{\partial^2 w^{(2)}}{\partial r^2}+r\dfrac{\partial w^{(2)}}{\partial r}-w^{(2)}=\dfrac{K_1 r^2\dfrac{\partial \Delta m}{\partial r}}{L_{22}} \\ \text{with, } K_1=L_{12}\beta_{11}+L_{23}\beta_{22}+L_{22}\beta_{22} \end{cases} \tag{8}$$

It is shown that the general solution of equation (8) writes as the sum of a solution of the homogeneous equation and of a particular solution.

$$
\begin{aligned}
w^{(2)}(r) = B^{(2)}r + \frac{C^{(2)}}{r} + \sum_{m=1}^{\infty} \frac{m_0 \pi \exp(-D\omega_m^2 t)}{J_0^2(b\omega_m) - J_1^2(a\omega_m)} J_1^2(a\omega_m) \frac{K_1}{L_{22}} \\
\Big[Y_0(b\omega_m) \sum_{k=0}^{\infty} \frac{(-1)^k (\frac{1}{2})^{2k+1} (\omega_m)^{2k+2}}{k!(k+1)!} \frac{r^{2k+3}}{((2k+3)^2 - 1)} - \frac{J_0(b\omega_m)}{\pi} \Big\{ \\
\sum_{k=0}^{\infty} \frac{(-1)^k (\frac{1}{2})^{2k+1} (\omega_m)^{2k+2}}{k!(k+1)!} [2\ln(\frac{1}{2}\omega_m) - \psi(k+1) - \psi(k+2)] \frac{r^{(2k+3)}}{((2k+3)^2 - 1)} + \\
2 \sum_{k=0}^{\infty} \frac{(-1)^k (\frac{1}{2})^{2k+1} (\omega_m)^{2k+2}}{k!(k+1)!} [\frac{\ln(r) r^{2k+3}}{((2k+3)^2 - 1)} - \frac{2(2k+3) r^{2k+3}}{((2k+3)^2 - 1)^2}] - r\ln(r) \Big\} \Big]
\end{aligned}
\tag{9}
$$

When the equilibrium state is reached, we retrieve in material 2 the displacement components previously proposed by Anifantis et al. [4]:

$$
\begin{cases}
u^{(2)}(x) = A^{(2)}x \\
w^{(2)}(r) = B^{(2)}r + \dfrac{C^{(2)}}{r}
\end{cases}
\tag{10}
$$

The preceding relations (10) stands for the displacement field in the material 1, at any time, with different constants, denoted $A^{(1)}$ and $B^{(1)}$, and the condition $C^{(1)}=0$ for the boundness of solution at r = 0 [3]:

$$
\begin{cases}
u^{(1)}(x) = A^{(1)}x \\
w^{(1)}(r) = B^{(1)}r
\end{cases}
\tag{11}
$$

Finally, the displacement field depends on five constants to be determined: $A^{(1)}$, $B^{(1)}$, $A^{(2)}, B^{(2)}$ and $C^{(2)}$. These five constants result from the following conditions:

- continuity of the displacement components at the interface

$$\begin{cases} u^{(1)}(a) = u^{(2)}(a) \\ w^{(1)}(a) = w^{(2)}(a) \end{cases} \tag{11}$$

- continuity of the radial stress at the interface and traction-free condition at the outer radii

$$\begin{cases} \sigma_{33}^{(1)}(a) = \sigma_{33}^{(2)}(a) \\ \sigma_{33}^{(2)}(b) = 0 \end{cases} \tag{12}$$

- global force balance of the cylinder

$$\int_0^a r\sigma_{xx}^{(1)} dr + \int_a^b r\sigma_{xx}^{(2)} dr = 0 \tag{13}$$

2.2. Example: on the use of optical fiber to measure the hygro-elastic mechanical state

Embedded optical Fiber Bragg Gratings (FBG) sensors have been proved to be well suited for strains measurements in composite materials [7-9]. Optical Fiber Bragg Gratings offer an indispensable tool to study, in a minimally invasive manner, internal strains in polymeric materials. A detailed stress analysis of the inclusion is required to correctly interpret the data from the fiber and on to the host material. The properties of the considered optical fiber (material 1) are presented in Table 1. The macroscopic properties of the considered composite (material 2) are presented in Table 2. The outer radius of the optical fiber *a* is 62.5 μm and the outer radius of the surrounding composite (material 2) *b* will be successively taken equal to 125, 250, 375, 500, 625 and 1250 μm which correspond to fiber volume fractions *Vf* of 25, 6.25, 2.78, 1.56, 1 and 0.25 % respectively.

Figures 2, 3 and 4 show the radial, hoop and axial stresses in the optical fiber and composite, as a function of r_{dim}, corresponding to a saturation state at 50% HR in the composite. Where

r_{dim} is the distance from the center of the optical fiber, normalized by the outer radius of the surrounding composite. Since a unidirectional composite at saturation state is considered, the hygro-elastic stresses must be null. High stress gradients occur in the region near to the optical fiber. Stress concentration in the vicinity of the optical fiber are caused by the heterogeneity of hygro-elastic properties between the composite and the optical fiber. The stress level in the fiber remains constant (i.e. it does not depend on the position). Up to a volume fraction of 2.78 %, the stresses in the optical fiber do not change, therefore the fiber is sufficiently far from the outer surface to be affected. The radial stress is continuous at the boundary between fiber and composite contrary to the case of the hoop and axial stresses. The radial stresses are tensile due to the swelling behaviour of the composite material resulting from the moisture absorption. Note that hygro-elastic stresses can negate thermal stresses induce by cooling [10]: the radial stresses due to the cooling should be compressive. The tensile radial stresses in the composite are balanced by the compressive axial and hoop stresses.

The stress field in the composite is more affected when the fiber volume fractions grows. Thus, in practice, an optical fiber having a small radius should be preferred, since this choice provides the weakest perturbation of the stress field in the studied composite material. Vacher [11], by a finite elements approach for steady-state thermoelastic problem, shows that the perturbations generated by the optical fiber are localized at a distance of twice its diameter. Table 3 presents the permanent hygro-elastic stresses, up to a volume fraction of 2.78 %, at a distance of twice the optical fiber diameter. At such a distance, the radial, hoop and axial stresses are close to the stresses (null) which arise without optical fiber. Besides, these stresses do still depend on the ratio between the fiber radius and composite radius.

Since the developed approach can take into account transient moisture state, the case of a fiber volume fraction of 1 % (a = 62.5 μm and b = 625 μm) is studied. For the considered composite material a relative humidity of 50 % induces a moisture content on the outer surface of 0.75 %. The transient moisture content and the corresponding radial, hoop and axial stresses are respectively depicted on Figures 5-8.

At the beginning of the diffusion process, the moisture content (Figure 5) shows strong gradients near to the outer surface. Then, the moisture diffuses through the whole composite cylinder, reducing the moisture content gradients. Eventually, an equilibrium state is reached in the composite part.

The radial stress gradients (Figure 6) in the vicinity of the optical fiber increase with time. In the first times, the moisture content gradients have a significant effect on the hoop and axial stresses (Figure 7 and 8). The transient analysis emphasizes, in the first times, the hoop and axial compressive states near to the external surfaces: compared to the permanent state, the transient state induces negative stress gradients for both the hoop and axial stresses. The maximum tensile hoop and axial stresses are reached during the diffusion process. This phenomenon is also encountered for the radial stress but at a certain distance from the optical fiber: as an example, at a distance of twice the optical fiber diameter (i.e. r_{dim} = 0.5). This behaviour is attended for unidirectional composite submitted to transient hygroscopic fields [12]. The hoop stress gradients in the vicinity of the optical fiber and the fiber stresses are growing functions of the time.

3. Three concentric cylinders

Consider three concentric cylinders (Figure 9), in which the central one is the transversely isotropic material 1 and the two others correspond to the transversely isotropic materials 2 and

3. Perfect interfacial bonding is assumed. The radius of material 1 is *a*, whereas the outer radii of materials 2 and 3 are r_0 and *b* respectively.

The diffusion in the ith layer is governed by equation (14), with initial dry conditions and external boundary moisture content m_0. The moisture fluxes are continuous at the boundary between material 2, denoted by the subscript $_2$, and material 3, denoted by the subscript $_3$. In addition, at the boundary between materials 2 and 3 the chemical potential is continuous but a moisture content jump is considered. The moisture content jump is characterised by a factor α denoting the ratio m_2^∞ / m_3^∞ of the saturation levels of the second layer (material 2) and the third layer (material 3) [13]. The material 1 is considered not to absorb water.

$$\frac{\partial m_i}{\partial t} = D_i \left[\frac{\partial^2 m_i}{\partial r^2} + \frac{1}{r}\frac{\partial m_i}{\partial r} \right] \quad a<r<b,\ t>0,\ \ i=2 \text{ to } 3 \tag{14}$$

$$\begin{cases} \dfrac{\partial m_2(a,t)}{\partial r} = 0 \\ m_2(r_0,t) = \alpha\, m_3(r_0,t) \\ D_2 \dfrac{\partial m_2(r_0,t)}{\partial r} = D_3 \dfrac{\partial m_3(r_0,t)}{\partial r} \\ m_3(b,t) = m_0 \\ m_i(r,0) = 0 \end{cases} \tag{15}$$

Applying the Laplace transform to system (14) and (15) and by using the residue theory to get the solution in the time space, we finally obtain the transient moisture content:

$$m_i(r,t) = m_i^\infty + \sum_{m=1}^{\infty} \frac{2\exp(-\omega^2{}_m t)}{\omega_m \Delta'_u(\omega_m)} \left\{ A_i J_0(\delta_i \omega_m r) + B_i Y_0(\delta_i \omega_m r) \right\} \tag{16}$$

$$\text{with } m_2^\infty = \alpha m_0 \text{ and } m_3^\infty = m_0$$

where J_0 and Y_0 are Bessel's functions of order zero, Δ_u is the determinant of 4*4 matrix $[a]$. A_i and B_i are determinants of matrices deduced from $[a]$ by respectively substituting column (2i-1) and 2i by the constant vector $\{g\}$. $\Delta'_u(\omega_m)$ is the derivative of Δ_u with respect to ω calculated for ω_m the mth positive root of Δ_u. δ_i are defined by the relations $\delta_i = \sqrt{1/D_i}$.

Furthermore, the non zero elements of $[a]$ and $\{g\}$ are:

$$a_{11} = D_2\delta_2\omega J_1(\delta_2\omega a),\ a_{12} = D_2\delta_2\omega Y_1(\delta_2\omega a)$$

$$a_{21} = J_0(\delta_2\omega r_0), a_{22} = Y_0(\delta_2\omega r_0),\ a_{23} = -\alpha J_0(\delta_3\omega r_0), a_{24} = -\alpha Y_0(\delta_3\omega r_0)$$

$$a_{31} = D_2\delta_2\omega J_1(\delta_2\omega r_0), a_{32} = D_2\delta_2\omega Y_1(\delta_2\omega r_0), a_{33} = -D_3\delta_3\omega J_1(\delta_3\omega r_0),$$

$$a_{34} = -D_3\delta_3\omega Y_1(\delta_3\omega r_0)$$

$$a_{43} = J_0(\delta_3\omega b), a_{44} = Y_0(\delta_3\omega b)$$

$$g_4 = c_0$$

3.1. Mechanical Problem

The mechanical states are deduced from the classical equations of solid mechanics (see *section 2.1.*). Since the central fiber does not absorb water, the relations (11) hold for the displacement field. In the materials 2 and 3 the displacement fields write as follows:

$$\begin{cases} u^{(i)}(x) = A^{(i)}x \\ A^{(i)} \text{ are constants.} \end{cases}$$

$$w^{(i)}(r) = B^{(i)}r + \frac{C^{(i)}}{r} - \sum_{m=1}^{\infty} \frac{2\exp(-\omega^2 m t)}{\omega_m \Delta'_u(\omega_m)} \frac{K_1}{L_{22}}$$

$$\Big[A_i \sum_{k=0}^{\infty} \frac{(-1)^k (\frac{1}{2})^{2k+1} (\delta_i \omega_m)^{2k+2}}{k!(k+1)!} \frac{r^{2k+3}}{((2k+3)^2 - 1)} + \frac{B_i}{\pi} \Big\{$$

$$\sum_{k=0}^{\infty} \frac{(-1)^k (\frac{1}{2})^{2k+1} (\delta_i \omega_m)^{2k+2}}{k!(k+1)!} [2\ln(\frac{1}{2}\delta_i \omega_m) - \psi(k+1) - \psi(k+2)] \frac{r^{(2k+3)}}{((2k+3)^2 - 1)} +$$

$$2 \sum_{k=0}^{\infty} \frac{(-1)^k (\frac{1}{2})^{2k+1} (\delta_i \omega_m)^{2k+2}}{k!(k+1)!} [\frac{\ln(r) r^{2k+3}}{((2k+3)^2 - 1)} - \frac{2(2k+3) r^{2k+3}}{((2k+3)^2 - 1)^2}] - r\ln(r) \Big\} \Big]$$

The unknown constants are deduced from the following conditions: continuity of the displacement components, continuity of the radial stress and traction-free condition at the outer radius, global force balance of the cylinder.

3.2. Example: presence of a neat resin interphase between the optical fiber and the composite

In practice, optical fibers are not completely surrounded by reinforcing fibers and a resin-rich layer, with material constant properties, between the optical fiber and the composite part can be considered. The outer radius of second layer, corresponding to the neat resin subdomain (material 2), is, for simplicity, chosen to be equal to twice the optical fiber radius (material 1). Now, we examine how the presence of a neat resin interphase affects the stress field. The properties of resin interphase are presented in Tables 4 and 5. The saturation levels of the

materials 2 and 3 (being the resin interphase and the composite, respectively) are presented in Table 6.

We notice the jump of moisture content at the boundary between the neat resin and the composite (Figure 10). Due to the neat resin subdomain, larger moisture contents than in the case of the two concentric cylinders are achieved.

High radial stress gradients take place in the resin region. This stress gradients are growing functions of the time. On Figure 11, we notice that a change of sign of the radial stress appears during the time in the resin and in the composite subdomains. Strong discontinuities appear for the hoop and axial stresses (Figure 12 and 13) at the boundaries between the interphase material, the optical fiber and the composite. Compared to the previous case, the presence of an interphase subdomain affects considerably the hoop and radial stress profiles and induces a reduction of the stresses in the optical fiber.

4. Conclusion

An analytical approach is investigated for transient hygro-elastic analysis of transversely isotropic multi-materials concentric cylinders. This approach allows to calculate the time and space dependent hygro-elastic stresses by applying the classical continuum mechanics formalism. Examples concerning embedded optical fiber, a pertinent way to measure internal strains, are given and thoroughly discussed. A detailed stress analysis of the inclusion (optical fiber) is required to correctly interpret the data from the fiber and on to the host material. The stress field perturbations induced by the intrusive optical fiber are evaluated and discussed. In particular, the role of the volume fraction of the optical fiber in the composite material is

considered. The influence of an interphase, here a neat resin subdomain, between the optical fiber and the composite is also pointed out. The proposed approach enables to calculate the local strain and stress field in composite materials submitted to transient hygroscopic fields. As an example, a carbon/epoxy composite material with impermeable carbon fibers can be considered: in that case, the model allows to calculate the time and space dependent stresses in the transversely isotropic carbon fibers, in the epoxy matrix and even in the interphases existing between the carbon fibers and matrix subdomains. In spite of the fact, that hygro-elastic problem only was considered in this study, such an approach can be extended to hygro-thermal problem combining thermal and hygroscopic loads.

References

[1] Lekhnitskii S. Theory of elasticity of an anisotropic body. Moscow: MIR Publishers, 1977.

[2] Nairn JA. Thermoelastic analysis of residual stresses in unidirectional high-performance composites. Polymer composites 1985; 6: 123-130.

[3] Wagner HD, Nairn JA. Residual thermal stresses in three concentric transversely isotropic cylinders: application to thermoplastic-matrix composites containing a transcrystalline interphase. Composite Science and Technology 1997; 57: 1289-1302.

[4] Anifantis NK, Kakavas PA, Papanicolaou GC. Thermal stress concentration due to imperfect adhesion in fiber-reinforced composites. Composite Science and Technology 1997; 57: 687-696.

[5] Kollar LP, Van Steenkiste RJ. Calculation of the stresses and strains in embedded fiber optic sensors. Journal of Composite Materials 1998; 32: 1647-1679.

[6] Crank J. The mathematics of diffusion. Oxford University Press, 1975.

[7] Botsis J, Humbert L, Colpo F, Giaccari P. Embedded fiber Bragg gratings sensor for internal strain measurements in polymeric materials. Optics and Lasers in Engineering 2005; 43: 491-510.

[8] Peters K, Studer M, Botsis J, Iocco A, Limberger H, Salathé R. Embedded optical fiber Bragg grating sensor in a nonuniform strain field: measurements and simulations. Experimental Mechanics 2002; 41: 19-28.

[9] Guemes JA, Menédez JM. Response of Bragg grating fiber-optic sensors when embedded in composite laminates. Composite Science and Technology 2002; 62: 959-966.

[10] Hahn HT, Kim RY. Swelling of composite laminates. Advanced Composite Materials Environnemental Effects ASTM STP 658 Vinson JR Ed. 1978; 98-120.

[11] Vacher S. Capteurs à fibres optiques pour le contrôle de l'élaboration et la caractérisation mécanique des matériaux composites. PhD Thesis, École des Mines de Saint-Étienne, 2004.

[12] Jacquemin F, Fréour S, Guillén R. A hygro-elastic self-consistent model for fiber-reinforced composites. Journal of Reinforced Plastics and Composites 2005; 24: 485-502.

[13] Jacquemin F, Vautrin A. Modelling of the moisture concentration field due to cyclical hygrothermal conditions in thick laminated pipes. European Journal of Mechanics A/Solids 2002; 21: 845-855.

[14] Tsai SW. Composite design. Third edition, Think Composites, 1987.

[15] Loos AC, Springer GS. Environmental effects on composite materials: Moisture absorption of graphite – epoxy composition immersed in liquids and in humid air. Technomic Publishing, Westport, USA, 1981. p. 34-55.

Figures

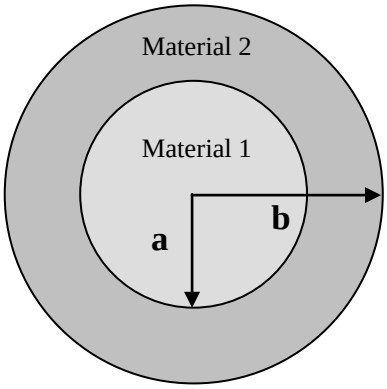

Figure 1. Cross-section of composite cylinder model.

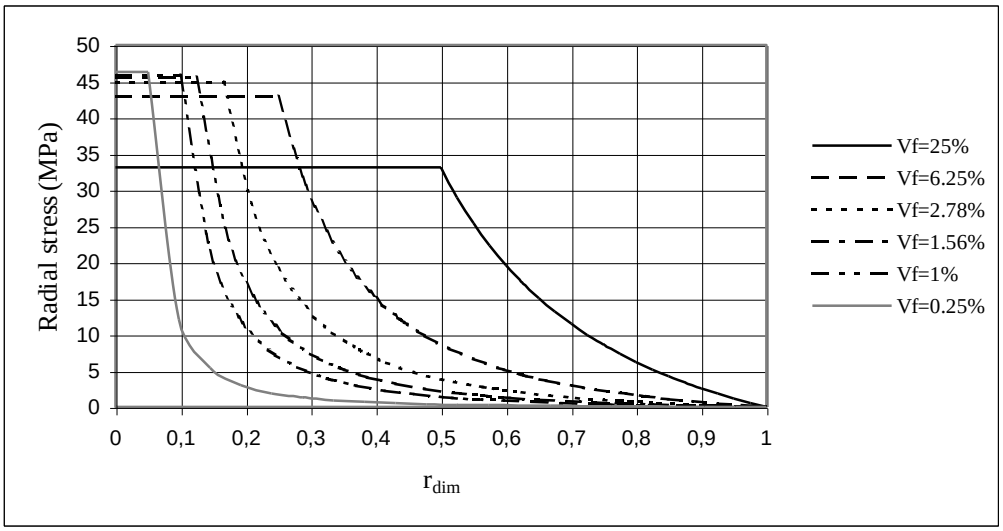

Figure 2. Radial stress versus fiber volume fraction in permanent state.

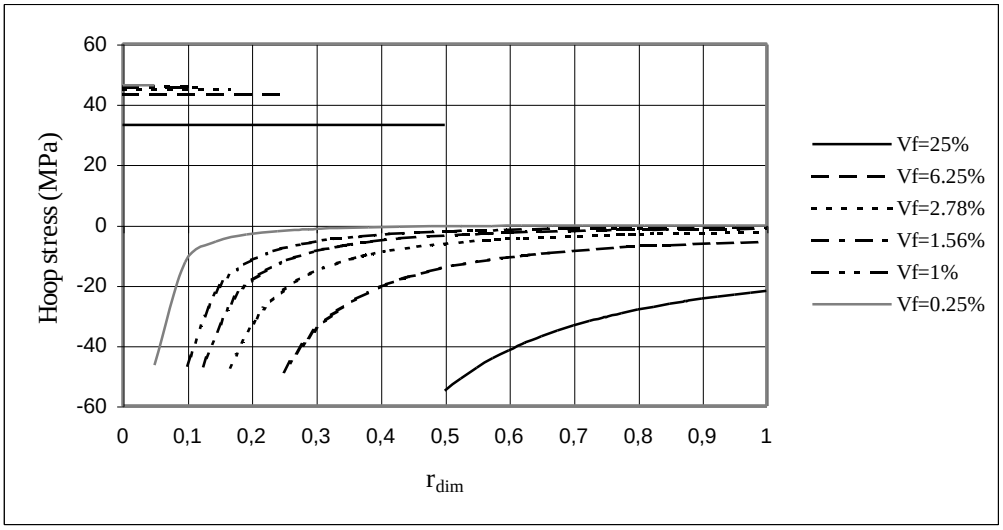

Figure 3. Hoop stress versus fiber volume fraction in permanent state.

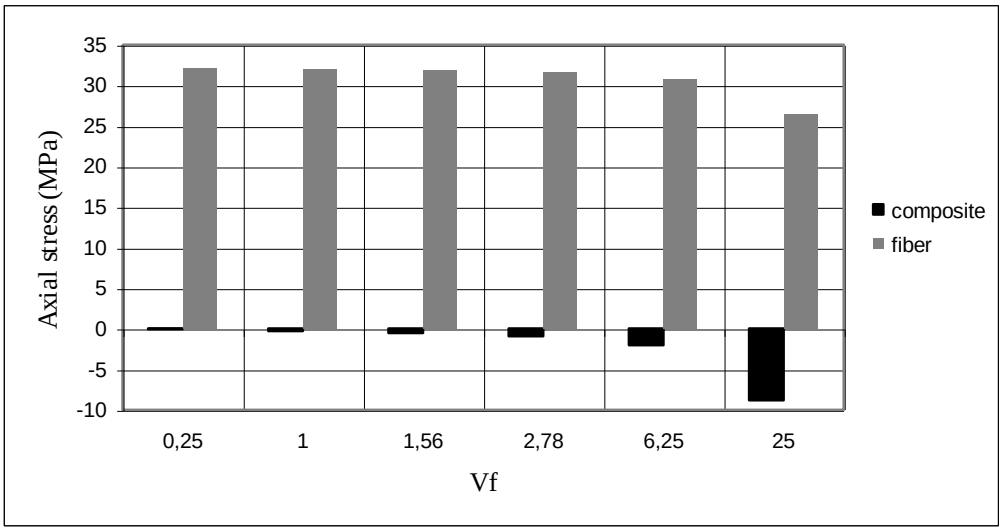

Figure 4. Axial stresses versus fiber volume fraction in permanent state.

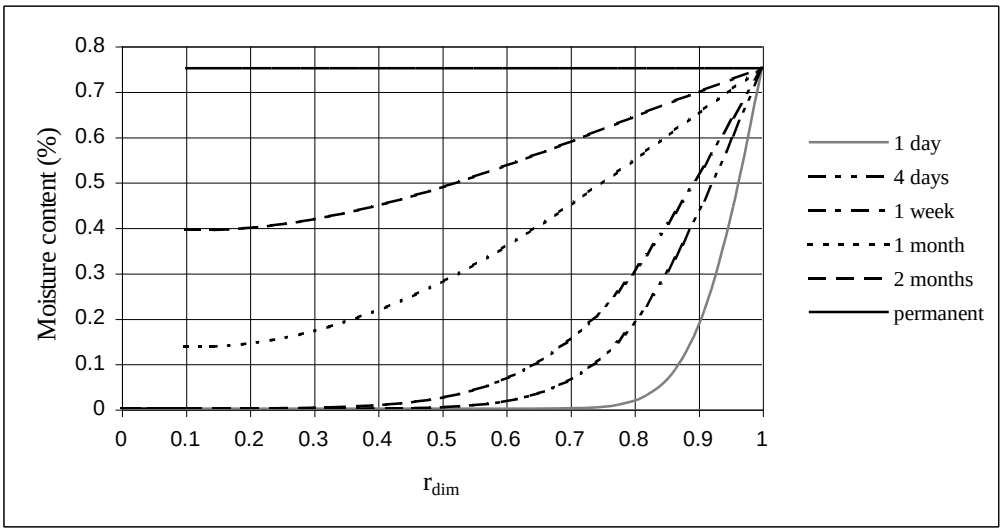

Figure 5. Transient moisture content (Vf =1%).

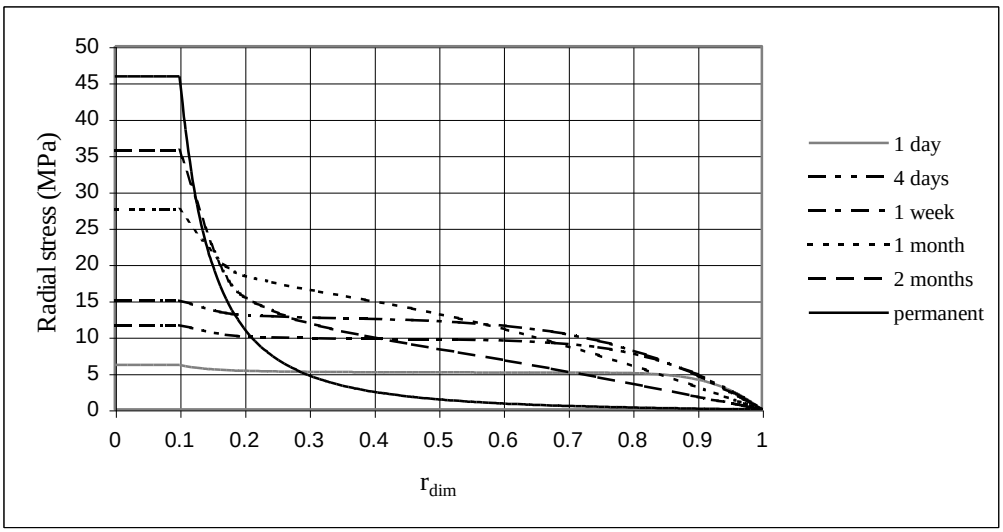

Figure 6. Radial stress in transient state (Vf =1%).

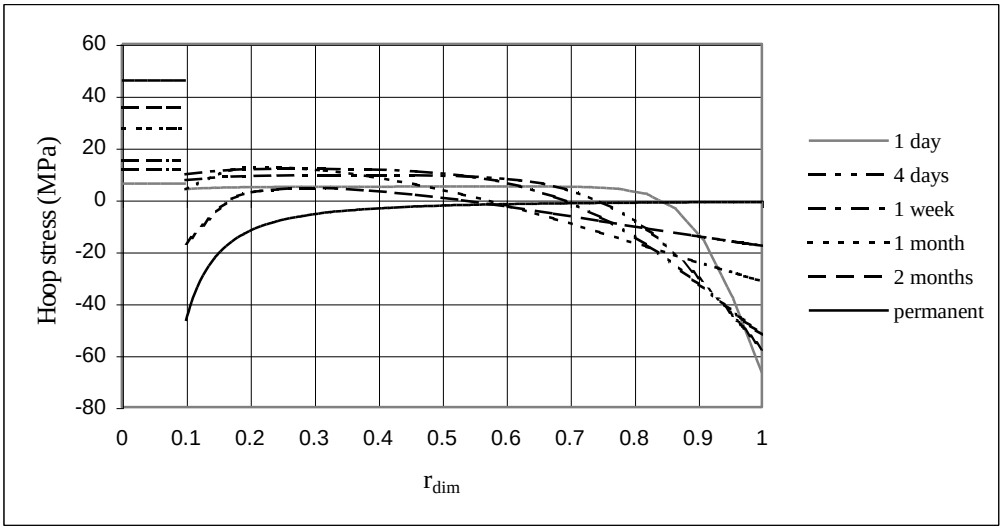

Figure 7. Hoop stress in transient state (Vf =1%).

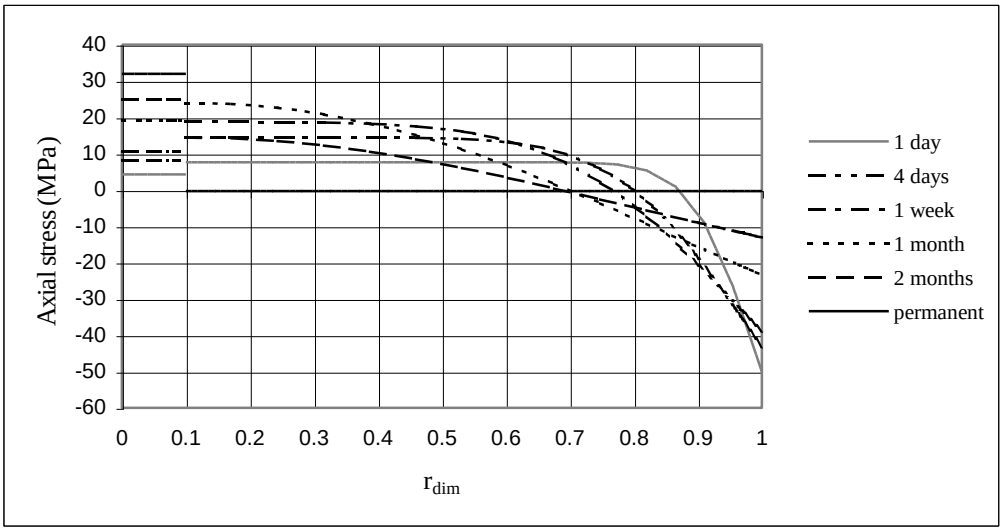

Figure 8. Axial stress in transient state (Vf =1%).

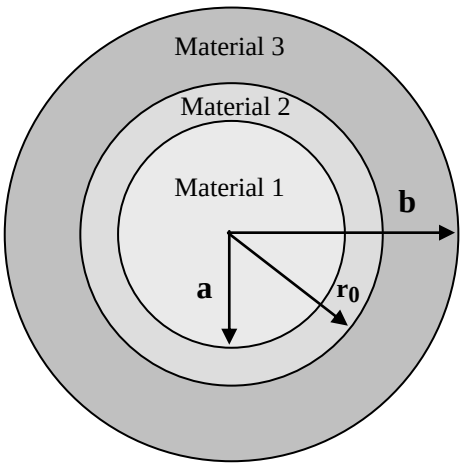

Figure 9. Cross-section of a three concentric cylinder composite model.

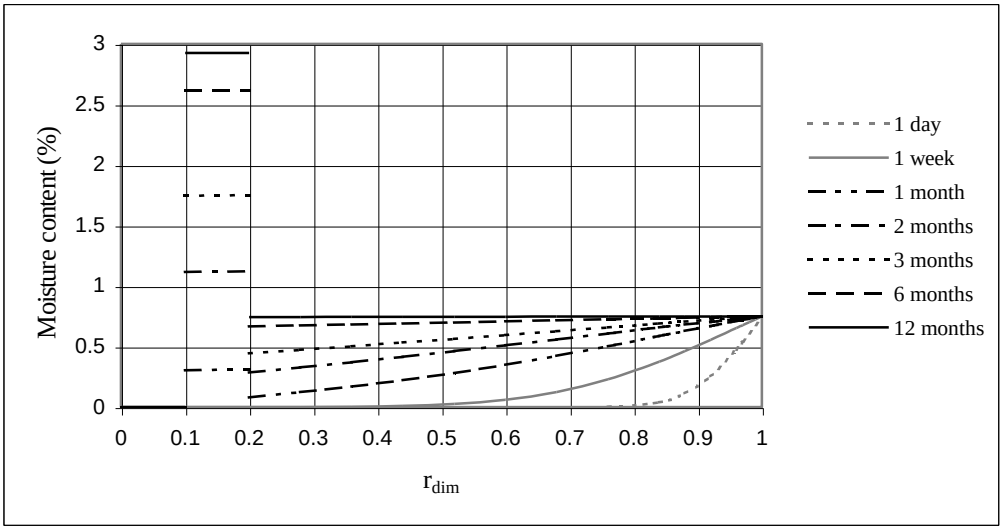

Figure 10. Transient moisture content for three concentric cylinders.

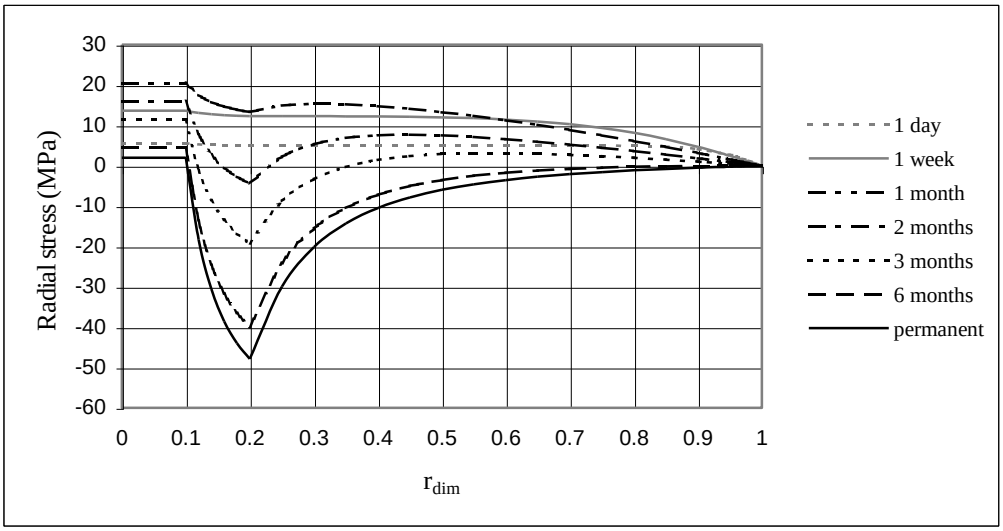

Figure 11. Radial stress in transient state for three concentric cylinders.

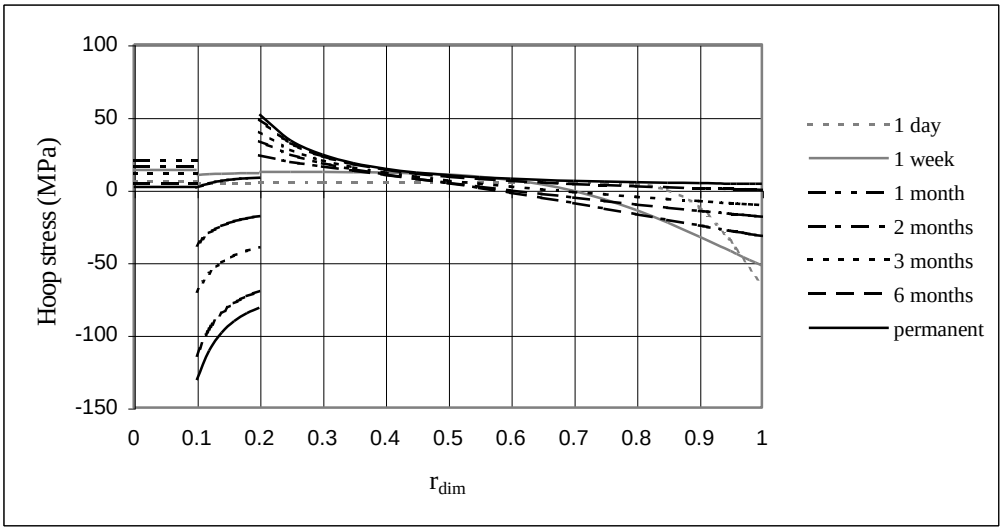

Figure 12. Hoop stress in transient state for three concentric cylinders.

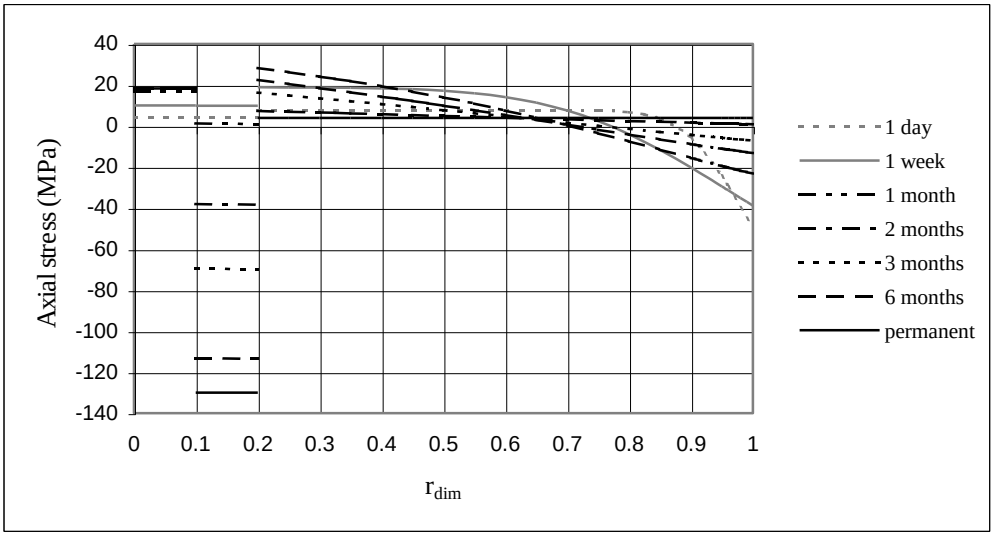

Figure 13. Axial stress in transient state for three concentric cylinders.

Tables

Properties	Values
Radius	62.5 μm
Young's modulus	73.1 GPa
Poisson's coefficient	0.17

Table 1. Properties of the optical fiber Corning SMF28 [11].

E_1 [GPa]	E_2, E_3 [GPa]	ν_{12}, ν_{13}	G_{23} [GPa]	G_{12} [GPa]	β_1	β_2, β_3
139.6	9.8	0.28	3.5	6.4	0.026	1.12

Table 2. Macroscopic hygro-elastic constants of a T300/5208 composite [12].

External radius *b* (μm)	Radial stress (MPa)	Hoop stress (MPa)	Axial stress (MPa)
375	0.56	-3.13	-0.90
500	1.13	-2.58	-0.50
625	1.35	-2.28	-0.32
1250	1.75	-1.98	-0.08

Table 3. Hygro-elastic stresses at a distance of twice optical fiber diameter.

E_1 [GPa]	E_2, E_3 [GPa]	ν_{12}, ν_{13}	G_{23} [GPa]	G_{12} [GPa]
4.5	4.5	0.4	1.6	1.6

Table 4. Mechanical properties of N5208 epoxy resin [14].

	β_{11}	β_{22}, β_{33}
N5208 epoxy matrix	0.6	0.6

Table 5. CME of the resin N5208 [14].

	N5208	T300/5208
m^{∞}	2.95 %	0.75 %

Table 6. Saturation levels at 50% HR [15].